# CONSTRAINT EFFECT ON THE FRACTURE BEHAVIOUR OF THE SIMULATED HEAT AFFECTED ZONE OF AN X-70 STEEL

**S. Rivera[1], R. Lezcano[1], C. Rodríguez[2], F.J. Belzunce[2] y C. Betegón[2]**

[1]Fundación ITMA, Centro Tecnológico del Acero y Materiales Metálicos, 33400 Avilés
E-mail: s.rivera@itma.es

[2] Escuela Politécnica de Ingeniería, Universidad de Oviedo, campus universitario, 33203 Gijón.
E-mail: cristina@uniovi.es

## ABSTRACT

The typical heat affected zone developed in an X-70 steel usually used to pipeline manufacture has been simulated via thermal treatment. A non-equilibrium microstructure consisting on ferrite, bainite and some martensite has been produced and characterized to have a much larger hardness and strength than the corresponding base metal but a lower ductility. Different single end notched bend specimens (SENB) with different crack lengths (a/W between 0.1 and 0.5) have been experimentally tested in order to assess the fracture behaviour of this product under different degrees of constraint. The J-Δa resistance curves at room temperature have been determined and the obtained results have been explained due to the effect of constraint on the ductile crack growth.

**KEY WORDS:** X-70 steel, constraint effect, elastoplastic fracture.

## 1. INTRODUCTION

Fracture assessment procedures play a key role in design, fabrication and fitness-for-service methodologies in the case of many engineering products as pipelines, pressure vessels, etc. Fracture mechanics approaches are based on the use of a single parameter, most commonly the J-integral or the crack tip opening displacement (CTOD), in the case of elastoplastic behaviour, which defines the crack driving force, to characterize the fracture resistance of the material. Current engineering flaw assessment methods make extensive use of these toughness parameters to define design curves which provide simplified and conservative criteria for fracture evaluation of structural components containing defects [1,2].

Conventional testing standards used to characterize the fracture resistance of metallic materials make always use of deeply cracked specimens in order to guarantee high crack tip constraint conditions and small scale yielding (SSY) levels. However, structural defects in pipelines and pressure vessels are very often surface cracks that generate in the course of fabrication, especially in the course of welding, or during in-service operation (slag and non metallic inclusions, corrosion damage, weld cracks, dents at weld seams, corrosion damage, etc). It is well known that these crack configurations generally develop low levels of crack-tip triaxiality which sharply contrast to conditions present in the standard deeply cracked specimens [3,4]. Consequently, predictions of fracture resistance based on standard deep cracked specimens may be in these cases unduly conservative and pessimistic and also can greatly increase the operational and maintenance costs.

There are different ways to define the crack-tip constraint. One of the most popular is the constraint ratio defined as the ratio between the hydrostatic stress to the Von Mises effective stress ($\sigma_h/\sigma_e$). Other constraint parameters are the T-stress [5,6] or the Q-parameter [7,8]. Whereas the T-stress is an elastic parameter which characterizes the geometrical constraint effect, the Q-parameter is a direct measure of the elastic-plastic stress fields that describes the deviation of the stress field, at a specified position ahead of the crack tip, from the reference stress distribution for which T=0 (SSY), which is fully accepted to be the general solution for a deep crack in an infinite specimen.

$$T = \frac{\beta K}{\sqrt{\pi a}} \tag{1}$$

$$Q = \frac{\sigma_{\theta\theta} - (\sigma_{\theta\theta})_{SSY,T=0}}{\sigma_{ys}} \quad \text{at } \theta=0,\ r = 2J/\sigma_{ys} \tag{2}$$

where $\beta$ is the biaxility parameter, dependent on the considered geometry, $K$ the corresponding stress intensity factor, $\sigma_{ys}$ the yield strength and $r$ and $\theta$ the polar coordinates taken from the crack tip. O`Dowd and Shih [7] demonstrated that, at least under small scale yielding, $Q$ and $T$ are univocally related.

It is so necessary to develop more accurate procedures for defect assessment when dealing with specific structures subjected to low levels of constraint. These approaches are based on the experimental testing of modified test specimens (shallow notch bend and tensile specimens) subjected to a constraint level that matches the one in the real structure.

## 2. EXPERIMENTAL PROCEDURE

A hot rolled plate of API X-70 Nb-V microalloyed steel with a final thickness of 15 mm has been employed. The plate was controlled rolled below the non-recrystallization temperature of the austenite and finally coiled at 547ºC. The chemical composition of the steel is shown in Table 1.

*Table 1. Chemical composition of the API X-70 plate*

| %C | %Mn | %Si | %S | %P | %Nb | %V |
|---|---|---|---|---|---|---|
| 0.12 | 1.55 | 0.23 | 0.003 | 0.017 | 0.049 | 0.060 |

As it is well known, the longitudinal welded joints produced during the manufacture of the pipeline represent the most critical region because small cracks and defects can appear and also the heat affected zones, especially the coarse grain region which attains a very high temperature, can be harder and have a much lower toughness.

The grain growth region of the heat affected zone produced when the plate is longitudinally welded to make the pipeline was simulated by means of a heat treatment. Several pieces of 200x120x15 $mm^3$ were quenched in water after austenitizing at 1100ºC during 40 minutes. The cooling rate at 700ºC at the centre of the thickness is about 80ºC/s, which matches well with the cooling rate produced when this steel is welded using a low heat input (1.8-2 $kJ/mm^2$) [9]. This point was assessed using the Rosenthal´s equation to determine the cooling rate in the weld heat affected zone for a three-dimensional heat flow [10]:

$$v = \frac{2\pi\lambda(T - T_0)}{H} \tag{3}$$

being $v$ the cooling rate at the temperature of interest $T_0$ (700ºC), $\lambda$ the workpiece thermal conductivity and $H$ the heat input.

The microstructure of the materials were analyzed using optical and scanning electron metallographies.

Tensile test specimens with a calibrated diameter of 10 mm were machined in the transversal direction of the plate and were tested at room temperature at a displacement rate of 3 mm/min.

Fracture toughness tests were performed using single edge notched bending (SENB) specimens, with a TS orientation and different crack length to width ratios (a/W = 0.1, 0.22 and 0.5), in order to get different levels of constraint. It is well known that as long as the deeply cracked SENB specimen (a/W=0.5) corresponds to a high crack-tip triaxiality, there is a progressive constraint loss as the a/W ratio of the SENB specimen decreases. The length of the specimens always corresponded with the transversal direction of the plate and their width and thickness were 14 mm.

Specimens were fatigue pre-cracked at ambient temperature to the required nominal a/W at an R-ratio of 0.1. Fracture tests were carried out at room temperature in accordance with the ASTM E1820 standard [11] using a load-line displacement rate between 0.2 and 0.4 mm/min.

The single-specimen method, based on the use of the elastic unloading compliance was employed to determine de J-Δa resistance curves and the obtained results were corrected using the physical measure of the crack determined at the end of each test by means of a suitable low magnification microscope [12].

The J integral was determined from the procedure developed by Sumpter for non-standard bending specimens [13] and improved by Joyce [14], which consists on splitting up its elastic and plastic components. The elastic component was obtained from the stress intensity factor, K, as:

$$J_e = \frac{K_i^2(a_i)(1-\upsilon^2)}{E} \tag{4}$$

and the plastic component is given by:

$$J_{pli} = \left[ J_{pl(i-1)} + \left( \frac{\eta_{i-1}}{b_{i-1}} \right) \frac{(P_i + P_{i-1})(v_{pli} - v_{pli-1})}{2B_N} \right] \cdot \left[ 1 - \gamma_{i-1} \frac{a_i - a_{i-1}}{b_{i-1}} \right] \tag{5}$$

being :

$$\eta_i = 0.32 + 12(a_i/W) - 49.5(a_i/W)^2 + 99.8(a_i/W)^3 \tag{6}$$

when $a_i/W < 0.282$, and

$$\gamma_i = -12.769 + 79.976(a_i/W) - 115.722(a_i/W)^2 \tag{7}$$

when $a/W < 0.325$

Otherwise, $\eta_i$ and $\gamma_i$ adopt the values given in the ASTM 1820 standard [11]. $P_i$ and $v_i$ are the applied load and the load-line displacement, $E$ and $\upsilon$ the elastic modulus and the Poisson ratio, $B_N$, $W$, $a$, the net thickness, width and crack length and $b_i=W-a_i$ [14].

Finally, the β parameter corresponding to the different SENB tested specimens was calculated using the following expression [16, 17]:

$$\beta = - 0.462 + 0.461\ (a/W) + 2.47\ (a/W)^2 \qquad (8)$$

Valid for $0.05 < a/W < 0.7$

## 3. RESULTS

Figures 1 and 2 show, respectively, the optical microstructure of the API X-70 plate and its simulated heat affected zone (HAZ). X-70 steel has a ferritic microstructure with only a small volume fraction of pearlite (about 3.3%). The ferritic grain size was between 11 to 12 ASTM (5-8 μm). The microstructure of the simulated heat affected zone consist manly in acicular bainite with some intergranular ferrite and small islands of martensite.

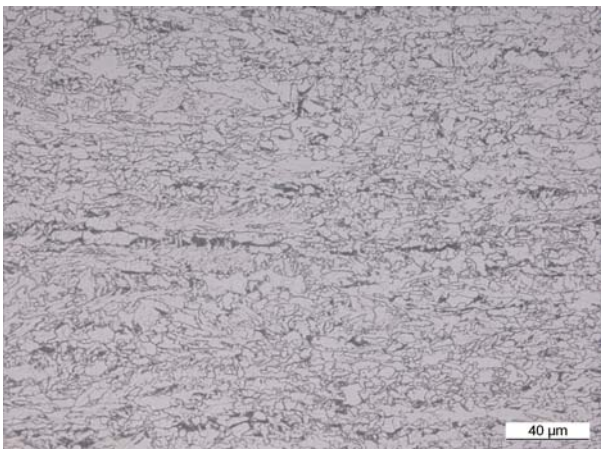


*Figure 1. API X-70 steel microstructure*

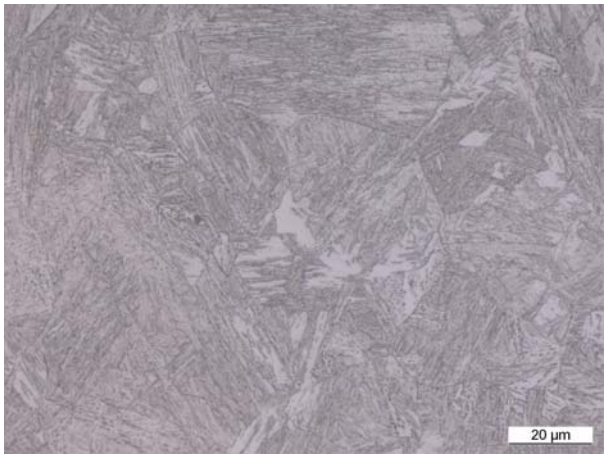


*Figure 2. Simulated heat affected zone microstructure*

The tensile mechanical properties and hardness of both materials, X-70 plate and its simulated heat affected zone, are presented in Table 2.
The simulated coarse grain heat affected zone has a much larger yield strength, ultimate tensile strength and hardness but a significant lower ductility than the original plate, as it could be expected.

*Table 2. Tensile mechanical properties and Vickers hardness*

| | $\sigma_{ys}$ (MPa) | $\sigma_u$ (MPa) | A (%) | HV |
|---|---|---|---|---|
| X-70 | 545 | 660 | 24 | 205 |
| Sim. HAZ | 905 | 1206 | 12.4 | 318 |

Figure 3 shows the load versus load line displacement plots experimentally obtained with SENB specimens with different a/W ratios (0.5, 0.22 and 0.1). All the specimens have exhibited an elastic-plastic behavior, and the tests were considered ended after a significant crack growth (determined by compliance measurement during unloading) was attained. Afterwards, the specimens were heat tinted and finally fully broken in order to measure the real values of the original crack length, $a$, and crack growth, $\Delta a$. These measurements were used to correct the $\Delta a$ values obtained by means of the already mentioned compliance technique.

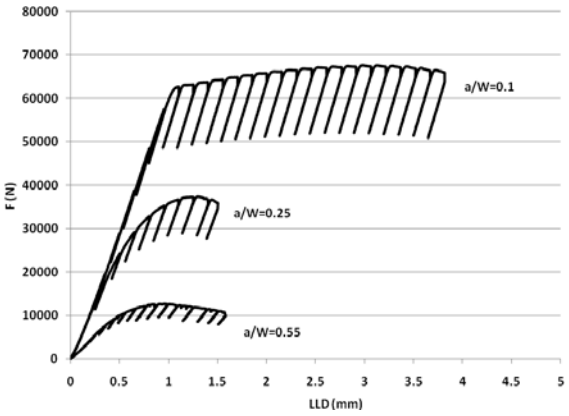


*Figure 3. SENB load versus load-line displacement plots corresponding to specimens with different a/W ratios*

Figure 4 shows the J-R curves experimentally obtained on the X-70 simulated coarse grain heat affected zone using the bend specimens with different a/W ratios.

The result obtained with the different geometries are clearly different and the expected constraint effect on crack growth is evident. The J initiation value, defined at a crack growth of 0.4 mm is about 200 kJ/m$^2$ for the deep cracked specimen but a twofold and threefold increase was observed respectively in the case of the specimens with shallow cracks (a/W=0.1, 0.22). The slope of the J-Δa curves also depends on the specimen geometry, hence the shorter cracks produce steeper J

crack growth resistance curves, and consequently, the differences of the measured J values among the tested geometries increase with the crack growth. For example the J values at crack extension of 0.6mm are approximately 260 kJ/m$^2$, 640 kJ/m$^2$ and 1000 kJ/m$^2$ respectively for a/W values of 0.5, 0.22 and 0.1. The same effect of constraint on the slope of the J resistance curves has been observed by different investigators in experiments made with a wide range of cracked geometries on several steels which failed in a ductile manner [14, 17].

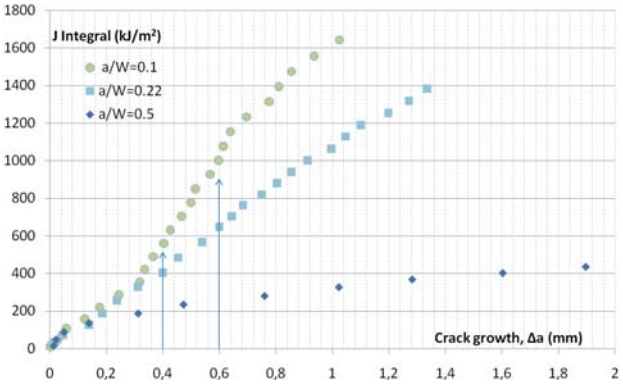


*Figure 4. J-R curves of simulated coarse grain HAZ for different a/W ratios*

## 4. DISCUSSION

Figure 5 shows the failure locus expressed as the $J_{0.4mm}$ and $J_{0,6mm}$ versus the normalized T-stress, $\tau$ ($\tau = T/\sigma_{ys}$) for the X-70 simulated coarse grain heat affected zone. The $\tau$ factor was obtained using expressions (1) and (8) with the K value corresponding to each case.

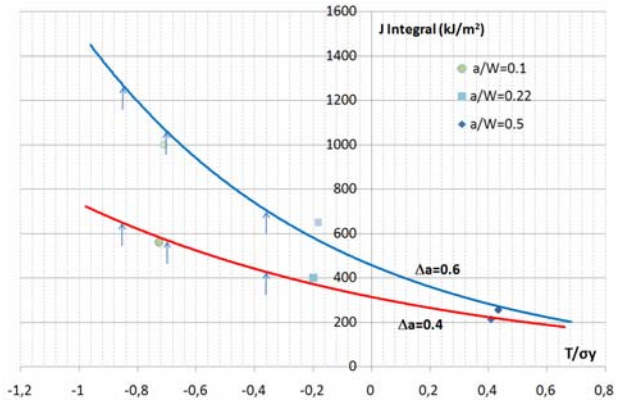


*Figure 5. J -τ failure locus of API X-70 simulated HAZ*

Figure 5 relates the evolution of the J resistance of this particular steel (coarse grain HAZ X-70 API steel) with the constraint factor, expressed by the elastic $\tau$ parameter. J values at crack growth initiation or after some particular crack growth are highly dependent on the geometry constraint, with larger J-values as $\tau$ is more negative (lower constraint).

In order to apply these results to the evaluation of pressurized pipelines, we have used the results published by Cravero and Ruggieri [3], which have made finite element analysis on axially cracked pipes. The analyzed geometries typify current trends in high pressure, high strength pipelines of high outside diameters (508 mm) and low thickness ($t$=12.7 mm). Typical external and internal surface flaws with a/t ratios 0.1, 0.25 and 0.5 were employed (crack depth, $a$ = 1.27mm, 3.175mm, and 6.35 mm, respectively).

Cravero and Ruggieri [3] also provide descriptions of crack-tip constraint in terms of *J-Q* trajectories for different axially cracked pressurized pipeline geometries and we have converted them in *J-τ*, making use of the polynomic relationship existing between these two parameters, which is represented in Figure 6 [18]. As it can be seen that this relationship is dependent on the materials constitutive law, we have used the curve which better matchs our own steel, $E/\sigma_y$=200.

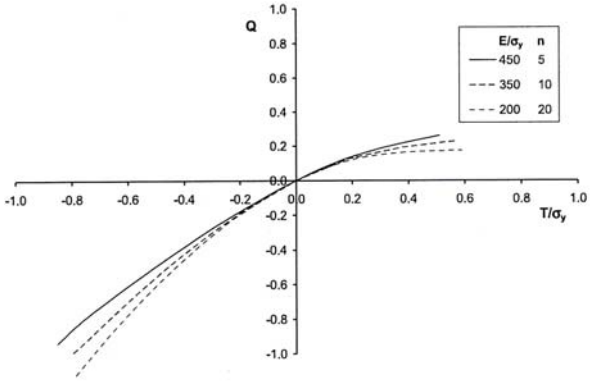


*Figure 6. Relationship between Q and τ for different constitutive equations*

The *J-τ* trajectories of the axially cracked pressurized pipelines with different crack sizes were also represented on Figure 5. The deep crack pipeline reveal a higher constraint loss than the deep notch SENB specimens, but the shallow crack pipelines exhibit much significant loss of constraint, which is even higher as the crack is shallower, but the crack location (internal or external) was demonstrate not to have influence on this point. Furthermore, the initial strong reduction in $\tau$ takes place when the global response of the specimen is still elastic, while the region with smaller change in $\tau$ with increasing J-levels confirms a fully plastic behaviour in the specimen.

It can be seen that in terms of constraint the deeply cracked pipeline ($a/t$ = 0.5) will attain at the failure load a triaxiality $\tau$ factor of -0.4, which can be well characterized by means of a SENB specimen with an $a/W$ ratio of 0.2 and the pressurized pipeline with $a/t$=0.2, will attain at fracture a triaxiality $\tau$ factor of

-0.7, which approximately corresponds to a SENB specimen with an *a/W* ratio of 0.1. Finally, when the pressurized pipeline has a very shallow crack (*a/t* = 0.1), the triaxiality factor at failure will be about -0.85 and this constraint value approximately corresponds to a SENB specimen with an *a/W* ratio lower than 0.1.

It can also be highlighted that the use of the critical *J* values obtained with the standard specimens (deeply cracked SENB specimens) give very low results, which give rise to unduly conservative and pessimistic expectations when they are used to predict the in-service failure of pressurized pipelines with real defects.

Nevertheless, the present study using an homogeneous microstructure corresponding to the simulated coarse grain heat affected region of an API X-70 steel is still conservative, as a real crack present in the coarse grain HAZ of an API X-70 pipeline will be embedded by the lower strength base steel, giving rise to an overmatched product (the yield strength of the region where the crack is located, the HAZ region, is larger than the yield strength of the base steel), which corresponds to a lower constraint configuration. This overmatching component behaves in the same way as an homogeneous material with a characteristic constraint parameter, so that mismatching and geometric effects can be simultaneously taken into account by the superposition of the normalized T-stresses, $\tau_m$, originated by the constraint due to material mismatching and $\tau_g$, originated by the geometrical constraint [19,20].

## 5. CONCLUSIONS

The typical coarse grain heat affected zone developed in an X-70 steel usually used to pipeline manufacture has been simulated via thermal treatment. A non-equilibrium microstructure consisting on ferrite, bainite and some martensite has been produced and characterized to have a much larger hardness and strength than the corresponding base metal but a lower ductility.

The effect of constraint on the J crack growth curves of the aforementioned simulated microstructure was studied by means of using SENB fracture specimens with different a/W ratios and the failure $J$-$\tau$ ($\tau = T/\sigma_y$) locus was also experimentally determined. SENB specimens with shallow cracks give always much higher initiation *J* values and resistant R-curves with a larger slope than the standard deep cracked specimens.

Representing the $J$-$\tau$ trajectories of axially cracked pressurized pipelines with different crack sizes on the studied steel biparametric failure locus, the necessity to find a SENB specimen with a crack depth with a constraint similar to that of the cracked pipe was demonstrated in order to assess the real fracture behavior of these structural components.

## 6. REFERENCES


[1] British Standard Institution, BS7910, *Guide on methods for assessing the acceptability of flaws in metallic structures*, 1999.

[2] American Petroleum Institute, API RP-579, *Recommended practice for fitness-for-service*, 2000.

[3] Cravero S and Ruggeri C., *Correlation of fracture behaviour in high pressure pipelines with axial flaws using constraint designed test specimens-Part I: Plane-strain analysis*, Engineering Fracture Mechanics, 72, 1344-1360, 2005

[4] Chiesa M. et al., *Efficient fracture assessment of pipelines. A constraint corrected SENT specimen approach*, Engineering Fracture Mechanics, 68, 527-547, 2001.

[5] A.M. Al-Ani. and J.W. Hancock J.W., *J-dominance of short cracks in tension and bending*, J. Mech. Phys. Solids, 39, 23-43, 1991

[6] C. Betegón and J.W. Hancock, *Two-parameter characterization pf elastic-plastic crack-tip fields*, J. Appl. Mech., 58, 104-110, 1991.

[7] N.P. O`Dowd and C.F. Shih, *Family of crack-tip fields characterized by a triaxiality parameter-I. Structures of fields*, J. Mech. Phys. Solids, 39, 989-1015, 1992

[8] N.P. O`Dowd and C.F. Shih, *Family of crack-tip fields characterized by a triaxiality parameter-II. Fracture applications*, J. Mech. Phys. Solids, 40, 939-963, 1992

[9] G. Heigt, H. Lengauer and P. Hodnik, *Heavy wall thermo-mechanically rolled plates for offshore construction use*, Steel Research Int., 79, 12, 931-937, 2008.

[10] S. Kou, Welding Metallurgy, Wiley Interscience, John Wiley & Sons Pub., 2003

[11] Tosal L, Rodríguez C, Belzunce F.J, Betegón C., *The influence of specimen size on the fracture behavior of a structural steel at different* temperatures, Journal of Testing and Evaluation, 28, N4, 276-281, 2000

[12] ASTM E1820 Standard, American Society for Testing and Materials, 1999.

[13] J.D.G. Sumpter, *Jc determination for shallow notch welded bend specimens*, Fatigue and Frac. Eng. Mat. & Struct., 10, 478, 1987

[14] X.K. Zhu and J.A. Joyce, *J-R resistance curve testing of HY80 steel using SE(B) specimens and normalization method*, Eng. Fract. Mech., 74, 2007, 2263.

[15] T.L. Sham, Rep. of the Dept. of Mech. Eng., Rensselaer Polytechnic Troy, 1989.

[16] M.T. Kirk, K.C. Koppenhoefer and C.F. Shih, *Effect of constraint on specimen dimensions needed to obtain structurally relevant toughness measures*, ASTM STP 1171, 1993, 79

[17] J.W Hancock, W.G Reuter and D.M Parkes, *Constraint and toughness parametrised by* T, ASTM Symposium, Indianapolis, 1991.

[18] A.H. Sherry, M.A. Wilkes, D.W. Beardsmore and D.P.G. Lidberg, *Material constraint parameters for the assessment of shallow defects in structural components. Part.I. Parameter solutions*, Eng. Fract. Mech., 72, 2005, 2373.

[19] C. Betegón and I. Peñuelas, *A constraint based parameter for quantifying the crack tip stress fields in welded joints*, Eng. Fract. Mech., 73, 2006, 1865

[20] M.C. Burstow, I.C. Howard and R.A. Ainsworth, *The influence of constraint on crack tip stress fields in strength mismatched welded joints*, J. Mech. Phys. Solids, 46, 1998, 845

## ACKNOWLEDGEMENTS

The authors acknowledge the support provided by FICYT (Principado de Asturias, Spain), Project FC-08-IB08-112C2.